Multicompartment Micelles from Polyester-Containing ABC Miktoarm Star Terpolymers

Naohiko Saito,[†] Chun Liu,[†] Timothy P. Lodge,*[,†,‡] and Marc A. Hillmyer*[,†]

Department of Chemistry and Department of Chemical Engineering and Materials Science, University of Minnesota, Minneapolis, Minnesota 55455

Received May 2, 2008; Revised Manuscript Received July 21, 2008

ABSTRACT: Well-defined μ-[poly(ethylethylene)][poly(ethylene oxide)][poly(γ-methyl-ε-caprolactone)] (μ-EOC) miktoarm star terpolymers were prepared by a combination of two successive living anionic polymerizations and one controlled ring-opening polymerization (ROP). A mid-hydroxyl-functionalized poly(ethylethylene)-*block*-poly(ethylene oxide) (PEE−PEO) diblock copolymer served as a macroinitiator for the aluminum-mediated ROP of γ-methyl-ε-caprolactone (MCL), leading to a family of μ-EOC triblock copolymers having monomodal molecular weight distributions and controlled PMCL weight fractions. Micelle structures formed in water from μ-EOC containing various lengths of PMCL were examined by cryogenic transmission electron microscopy (cryo-TEM) and dynamic light scattering. Increasing the fraction of hydrophobic PMCL resulted in a transition from spherical to wormlike to approximately spherical micelles. Although the multicompartment cores of the μ-EOC micelles could not be directly resolved by cryo-TEM, small-angle X-ray scattering analysis of a representative PEE−PMCL diblock copolymer showed clear microphase separation, strongly suggesting the existence of multicompartment cores in the μ-EOC micelles. We speculate that the transition of μ-EOC micelles from worms to spheres can be attributed to the connection of the three immiscible blocks at one junction and documented micellar transitions in analogous PMCL−PEO diblock micelles.

Introduction

Multicompartment micelles are recently discovered nanoscopic aggregates with subdivided solvophobic cores.[1−3] Whereas AB diblock copolymer micelles are limited to the partitioning of space into "inside" and "outside", multicompartment micelles have more complex core structures. Two or more distinct core domains could be used to store two or more incompatible agents in nanocompartments of the core.[4] Ideally, multicompartment micelles could be used to transport and deliver combinations of pharmaceutical agents concurrently in a desired stoichiometric ratio.

To date, most work regarding multicompartment micelles has focused on linear multiblock polymer systems. Those micelle structures typically feature a concentric core−shell−corona arrangement of domains, regardless of the overall micelle shape. For example, Yu and Eisenberg reported the formation of spherical, rodlike, and vesicular aggregates of polystyrene-*b*-poly(methyl methacrylate)-*b*-poly(acrylic acid) (PS−PMMA−PAA) in a mixture of an organic solvent (e.g., dioxane, THF, and DMF) and water.[5] Gohy et al. prepared pH-responsive core−shell−corona micelles of PS-*b*-poly(2-vinylpyridine)-*b*-poly(ethylene oxide) (PS−P2VP−PEO) and showed the reversible contraction and expansion of the P2VP shell by changing the pH.[6−9] Zhou et al. observed disklike core−shell−corona micelles from linear ABC triblocks consisting of a fluorinated polybutadiene (PBD) derivative, PS, and PEO.[10] Pochan, Wooley, and co-workers systematically studied the formation of toroidal, disklike, and wormlike assemblies of PS-*b*-poly(methyl acrylate)-*b*-PAA (PS−PMA−PAA) by controlling the level of a diamine additive and the solvent composition (THF and water).[11−16] Kubowicz et al. observed multicompartment "raspberry-like" cores consisting of small spheres within a matrix in micelles of poly(4-methyl-4-(4-vinylbenzyl)morpholin-4-ium chloride)-*b*-PS-*b*-poly(pentafluorophenyl 4-vinylbenzyl ether) (PVBM−PS−PVBFP).[17] In their case, the micelles did not adopt a core−shell−corona arrangement. They concluded that the small spheres in the core comprise only the fluorocarbon moieties of PVBFP (i.e., not the entire PVBFP blocks), while the matrix consisted of PS and the hydrocarbon component of PVBFP. Recently, Thünemann et al. explored the self-assembly of two-compartment cylindrical micelles formed from an ABCBA pentablock polymer consisting of PEO, poly(γ-benzyl L-glutamate), and a perfluoropolyether in aqueous solution.[18] These micelles appeared to have a core−shell−corona morphology due to the strong segregation between the fluorocarbon and the oligopeptide.

A relatively small number of reports have been published investigating the aqueous self-assembly of miktoarm (μ) ABC star terpolymers with multicomponent cores,[19] though many groups have reported synthetic protocols for well-defined μ-ABC star terpolymers.[20−29] Over the past few years we have focused on the synthesis and self-assembly of this class of materials. Using well-defined μ-[poly(ethylethylene)][PEO][poly(perfluoropropylene oxide)] (μ-EOF) miktoarm star triblock copolymers (synthesized by two successive anionic polymerizations and one polymer−polymer coupling reaction[30,31]), we documented the formation of multicompartment micelles by using cryogenic transmission electron microscopy (cryo-TEM).[1] The aqueous self-assembly of μ-EOF resulted in the formation of several new multicompartment micellar structures, depending on the relative lengths of the blocks.[32−34] At large fractions of PEO, a flat poly(perfluoropropylene oxide) (PFPO) phase was sandwiched by two poly(ethylethylene) (PEE) layers, leading to the formation of hamburger or segmented wormlike micelles in water.[34] With decreasing PEO fraction, μ-EOF micelles formed nanostructured bilayers and vesicles with PFPO domains dispersed in a PEE matrix.[33] We also observed the formation of spherical raspberry-like micelles and multicompartmentalized worms induced by an increase in the superhydrophobic and oleophobic PFPO fraction.[32] These structures can be understood through the interplay of several factors: the mandatory convergence of the three immiscible blocks, the high incompatibility between PEE and PFPO even at modest molecular weight, and

* To whom correspondence should be addressed. E-mail: hillmyer@umn.edu (H.A.M.); lodge@umn.edu (T.P.L.).
† Department of Chemistry.
‡ Department of Chemical Engineering and Materials Science.

10.1021/ma801001s CCC: $40.75
Published on Web 10/22/2008

the extreme incompatibility of the PFPO block with the solvated PEO block. We hypothesize that these systems lie in the superstrong segregation regime (SSSR), where the interfacial tension between the core and corona + solvent is so large that the core-forming block is essentially fully stretched to minimize the interfacial area per chain.[35,64]

Multicompartment micelles have mostly been investigated using a core composed of hydrocarbon and fluorocarbon moieties due to their strong incompatibility. Here we report the synthesis of polyester-containing μ-ABC triblocks consisting of PEE, PEO, and poly(γ-methyl-ε-caprolactone) (PMCL) and their self-assembly in water. By incorporating PMCL, biomedical applications of such structures could be realized given the degradation and biocompatibility characteristics of such aliphatic polyesters.[36] While the segregation strength between PEE and PMCL is likely weaker than that for PEE and PFPO, the combination of a polyester and polyolefin can exhibit a rather large Flory−Huggins interaction parameter χ; thus, the polyester/polyolefin combination should be microphase-segregated at modest molecular weight relative to other polymer pairs comprising hydrocarbon backbones. For example, χ values for PS-*b*-poly(D,L-lactide) (PS-*b*-PLA) and poly(ethylene-*alt*-propylene)-*b*-poly(D,L-lactide) (PEP-*b*-PLA) are reported to be 0.22 and 0.85 at 298 K, respectively.[37,38] For comparison, χ for polystyrene and polyisoprene is about 0.06 at the same temperature.[39]

Experimental Section

Materials. A mid-hydroxyl-functionalized PEE-PEO diblock copolymer previously synthesized and characterized was used as a precursor for preparation of μ-PEE−PEO−PMCL (μ-EOC).[30] The molar masses of PEE and PEO in the diblock are 2 and 9 kg/mol, respectively, and the polydispersity index (PDI) (M_w/M_n) as determined by size exclusion chromatography (SEC) is 1.09. THF was purified by being passed through an activated alumina column using a home-built solvent purification line.[40] Pyridine was dried over calcium hydride and was distilled prior to use. Triethylaluminum (1.0 M in heptane), 4-methylcyclohexanone (99%), and 3-chloroperbenzoic acid (mCPBA) were used as received (Aldrich). Butadiene (Aldrich, 99.8%) (BD) was vacuum-distilled from *n*-butyllithium after being stirred in a sealed flask for 2 h at −20 °C. Ethylene oxide (Aldrich, 99.5%) (EO) was vacuum-distilled from *n*-butylmagnesium chloride after being stirred in a sealed flask at 1 h at 0 °C. *sec*-Butyllithium (Aldrich, 1.23 M in cyclohexane) (*sec*-BuLi) was used as received.

γ-methyl-ε-caprolactone (MCL) was prepared by the Baeyer−Villiger oxidation of 4-methylcyclohexanone in the presence of 1.4 equiv of mCPBA in CH_2Cl_2 [ca. 5% (w/v) solution] at 25 °C for 24 h.[41−43] The *m*-chlorobenzoic acid byproduct was removed by repeated filtration until no precipitate was present when the solution was cooled to −78 °C. The mixture was subsequently washed with saturated $NaHCO_3$ three times and once with NaCl aqueous solution and dried over $MgSO_4$. The crude solution was filtered through a plug of silica gel, concentrated on a rotary evaporator, and subsequently vacuum-distilled over calcium hydride prior to use. The yield was 64%, and the ^{1}H NMR spectrum of MCL corresponds to that in a previous paper.[43]

Preparation of μ-EOC. Mid-hydroxyl-functionalized PEE-*b*-PEO was dried by two azeotropic distillations in toluene and dried in vacuo overnight at 90 °C before use. PEE-*b*-PEO, THF, 1.1 equiv of triethylaluminum, and 3 equiv of pyridine with respect to polymer were added to the flask under N_2. The sealed flask was placed in an oil bath at 60 °C for 1 h. MCL (1−2 M in THF) was subsequently added to the macroinitiator solution, and the polymerization was carried out at 60 °C for 15−20 min (Scheme 1). Polymerization was quenched by addition of HCl (1 M methanol/water = 50/50, w/w), and the product was precipitated in petroleum ether or 2-propanol to remove any unreacted MCL. The polymer was redissolved in CH_2Cl_2, dried over $MgSO_4$, filtered, centrifuged, decanted, concentrated and dried in vacuo overnight. Four μ-EOC(2−9−*x*) samples having different chain lengths of MCL were prepared and are listed in Table 1, where the numbers correspond to the molar masses (kg/mol) of PEE, PEO, and PMCL blocks, respectively.

Scheme 1. Synthetic Route to μ-PEE−PEO−PMCL Star Terpolymers

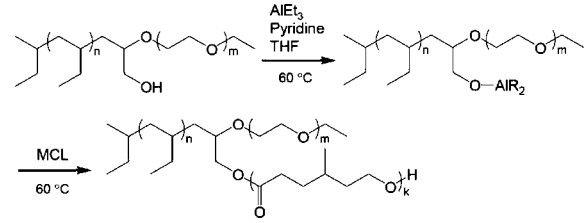

Table 1. PEE-*b*-PEO and μ-PEE−PEO−PMCL Molecular Parameters

sample ID[a]	N_{PEE}[b]	N_{PEO}	N_{PMCL}[c]	w_{PEE}[d]	w_{PEO}	w_{PMCL}	M_n[c] (kg/mol)	PDI[e]
EO(2−9)[f]	31	197		0.17	0.83		10.6	1.09
μ-EOC(2−9−2)	31	197	14	0.14	0.71	0.15	12.4	1.14
μ-EOC(2−9−4)	31	197	34	0.12	0.59	0.29	15.0	1.17
μ-EOC(2−9−8)	31	197	64	0.09	0.47	0.44	18.8	1.22
μ-EOC(2−9−12)	31	197	93	0.08	0.39	0.53	22.5	1.33

[a] The numbers after the sample name correspond to the molar masses (kg/mol) of PEE, PEO, and PMCL blocks, respectively. [b] *N* denotes the degree of polymerization of the polymer. [c] Measured by ^{1}H NMR spectroscopy in $CDCl_3$. [d] *w* denotes the weight fraction of the polymer. [e] Determined by SEC using PS standards and $CHCl_3$ as an eluent at 35 °C. [f] Previously prepared and characterized.[30]

μ-EOC micelles were prepared in two different ways. (i) Thin film hydration technique (see ref 43): μ-EOC was first dissolved in CH_2Cl_2, and the solvent was evaporated at room temperature in a glass vial, yielding thin polymer films on the sides of the vials. Residual solvent was removed in vacuo overnight. An appropriate amount of deionized water was added to the vial, and the solution (1 wt % polymer in water) was stirred for at least 1 week at room temperature prior to further analysis. Most polymers dispersed in a few hours by visual inspection. (ii) Dialysis technique (see ref 44): μ-EOC was first dissolved in THF (1 wt % polymer in THF), and deionized water was slowly added to the polymer/THF solution (at a rate of 1 drop every 30 s) with vigorous stirring (PEE, PEO, and PMCL are all soluble in THF). As the water content increased, the solubility of both PEE and PMCL decreased, resulting in the formation of micelles as indicated by the appearance of turbidity in the solution. The slow addition of water continued until 60−80 wt % water content had been achieved. For μ-EOC(2−9−8) and μ-EOC(2−9−12), the turbidity appeared at water contents of 25−30 wt %, whereas the micelle solutions of EO(2−9), μ-EOC(2−9−2), and μ-EOC(2−9−4) did not show any turbidity change due to the small size of the micelles formed. All micelle solutions were then placed in dialysis tubes (Spectra/Por, molecular weight cutoff 2000) and dialyzed against deionized water to remove THF. Deionized water was changed twice a day for 5 days. After dialysis, the polymer/water solutions were adjusted to 0.5 wt % by adding or removing water (by evaporation with a N_2 purge) and stirred for at least 1 week at room temperature prior to further analysis.

Preparation of PEE-*b*-PMCL. A procedure for preparation of hydroxyl-end-functionalized PEE (PEE−OH) is briefly described below. A more detailed description of the equipment and general procedures can be found elsewhere.[45] The polymerization was performed in a 2 L round-bottom glass reactor fitted with five ACE-THREADS connectors containing a glass-coated magnetic stir bar. The reactor was flame-dried and evacuated to 30 mTorr overnight. Purified THF (500 mL) was added, and the reactor was cooled to −60 ± 5 °C with a dry ice/2-propanol bath. *sec*-BuLi (6.7 mmol) was injected, causing the reaction mixture to become yellow. Purified BD (0.25 mol) was added 15 min after the addition of *sec*-BuLi. The reaction mixture was stirred for 5 h at −60 ± 5 °C

and quenched with purified EO (0.1 mol), causing the mixture became to colorless. The reaction mixture was stirred for 1 h and slowly warmed to room temperature before addition of degassed methanol. The crude product solution was concentrated on a rotary evaporator and redissolved in 500 mL of cyclohexane. The solution was washed with deionized water four times, concentrated, redissolved in THF, and subsequently precipitated into methanol. The product was dried under reduced pressure for 1 week at room temperature.

Hydrogenation of end-functionalized PBD was performed in cyclohexane in a high-pressure stainless steel reactor. The PBD homopolymer solution with a concentration of 20 g/L was purged with argon for 30 min before hydrogenation. Pd on calcium carbonate (Aldrich, 5 wt %) was used as the catalyst in the same amount as the PBD precursor by weight. The catalyst was first heated to 80 °C under vacuum for 2 h in the reactor and subsequently reduced under 100 psig of H_2 for 2 h. The pressure in the reactor was reduced to 10 psig, and the PBD solution was added to the reactor by pressure-driven flow (Ar). The reaction was performed under 500 psi of H_2 at 80 °C for 24 h. After the reaction the reactor was cooled to room temperature, and the catalyst was removed from the crude product by filtration. The polymer solution was subsequently concentrated on a rotary evaporator and dried under vacuum until the weight remained constant.

Polymerization of MCL using PEE−OH as a precursor was carried out in the same manner as described above for preparation of μ-EOC. MCL was polymerized by aluminum-mediated ring-opening polymerization (ROP) with the PEE−OH using triethylaluminum and pyridine in THF. Purification of PEE-*b*-PMCL was also carried out in the same manner as described above. The scheme for preparation of PEE-*b*-PMCL is shown in Figure S1, Supporting Information.

Molecular Characterization. ^{1}H NMR spectra were collected on a Varian INOVA-300 or Varian INOVA-500 spectrometer at room temperature. All samples were dissolved in $CDCl_3$. PDIs were determined by SEC on a Hewlett-Packard 1100 series liquid chromatograph fitted with a Hewlett-Packard 1047A refractive index detector and three PLgel columns and calibrated with polystyrene standards (Polymer Laboratories). Chloroform was used as an eluent at a flow rate of 1 mL/min at 35 °C.

Cryo-TEM. Cryo-TEM samples were prepared in a controlled environment vitrification system (CEVS) at room temperature.[46] An aliquot of the micelle solution was placed onto a lacey carbon-supported TEM grid, which was held by tweezers and suspended in the aqueous-vapor-saturated chamber of the CEVS. Excess solution was removed through blotting with a piece of filter paper, resulting in a formation of films with thicknesses of ca. 100−300 nm in the mesh holes. After at least 20 s was allowed for relaxation of any stresses induced during the blotting, the samples were quickly plunged into a reservoir of liquid ethane cooled by liquid nitrogen. Vitrified specimens, which were stored in liquid nitrogen prior to being transferred and mounted on a cryogenic sample holder (Gatan 626), were observed with a JEOL 1210 TEM instrument operated at an acceleration voltage of 120 kV at about −178 °C. Images were recorded on a Gatan 724 multiscan CCD camera and processed with Digital Micrographs version 3.3.1. The phase contrast was enhanced by acquiring images at underfocus.

Dynamic Light Scattering (DLS). Samples for DLS were prepared by filtering the solutions through 0.45 μm hydrophilic filters into dust-free 0.25 in. diameter glass tubes. DLS measurements were performed using a Lexel model 75 Ar^+ ion laser with an operating wavelength (λ) of 488 nm and a home-built goniometer with a temperature-controlled silicon oil bath. The scattered light intensity was detected using a Brookhaven BI-DS photomultiplier and processed using a digital correlator (BI-9000AT). Intensity autocorrelation functions, $g_2(\tau)$, were measured at six different scattering angles between 45° and 120° at 25 °C. The electric field correlation functions, $g_1(\tau)$, were obtained from the measured intensity correlation functions by using the Siegert relation $g_2(\tau) = 1 + \beta|\, g_1(\tau)|^2$, where $0 \le \beta \le 1$ is the spatial coherence factor. These functions were analyzed using cumulant and double-exponential fits. Cumulant fitting gives information about the micelle size distribution (mean and width) for a monomodal distribution. The following cumulant expansion was used to fit the data:[47,48]

$$g_1(\tau) = A \exp(-\Gamma\tau)\left(1 + \frac{\mu_2}{2!}\tau^2 - \frac{\mu_3}{3!}\tau^3\right) \quad (1)$$

where Γ is the mean decay rate and μ_2 and μ_3 are second and third cumulants, respectively. μ_2/Γ^2 is used as a measure of the relative width of the size distribution. For double-exponential fits, which are utilized for a system exhibiting two distinct decay modes, the following function was used:

$$g_1(\tau) = A_1 \exp(-\Gamma_1\tau) + A_2 \exp(-\Gamma_2\tau) \quad (2)$$

where A_1 and A_2 represent the relative contributions to the scattered field of the decay rates Γ_1 and Γ_2. Using either eq 1 or eq 2, Γ was determined for different wave vector values [$q = 4\pi n\lambda^{-1} \sin(\theta/2)$, where n is refractive index of the solvent and θ is the scattering angle]. The mean diffusion coefficient D was determined by a linear fit of the mean decay rate Γ vs q^2 with an imposed zero intercept, where $\Gamma = Dq^2$ (see the inset in Figure S2, Supporting Information). The effective hydrodynamic radius, R_h, was determined using the Stokes−Einstein equation ($R_h = k_BT/6\pi\eta D$, where k_B, T, and η are the Boltzmann constant, absolute temperature, and solvent viscosity, respectively). Inverse Laplace transformations of the electric field correlation functions were also performed using the constrained regularization program REPES to obtain the distribution of relaxation times, which reflects the size distribution of the micelles.[49]

Small-Angle X-ray Scattering (SAXS). SAXS measurements for PEE-*b*-PMCL were performed at the University of Minnesota using Cu Kα X-rays (λ = 1.542 Å) generated by a Rigaku RU-200BVH rotating anode fitted with a 0.2 × 2 mm^2 microfocus cathode and Franks mirror optics. Azimuthally isotropic two-dimensional scattering patterns were integrated to one-dimensional plots of the intensity vs scattering wave vector q.

Results

μ-EOC was prepared by the ROP of MCL initiated by an aluminum alkoxide group installed at the block junction of PEE-*b*-PEO. The functionality of the hydroxyl group at the junction of the PEE and PEO blocks was confirmed previously by reaction with 1-naphthyl isocyanate, a hydroxyl-reactive fluorescent label.[30] Pyridine was used as a Lewis base in the ROP of MCL, since Vangeyte and Jerome proposed PEO chains might have a chelating effect toward aluminum and prevent monomer insertion, leading to the polymer having a bimodal molecular weight distribution.[42] Figure 1 shows the SEC traces of PEE-*b*-PEO and μ-EOC with different PMCL chain lengths. With increasing monomer-to-initiator molar ratio, the SEC profiles of μ-EOC continuously shifted toward lower elution volumes while narrow molecular weight distributions were retained. μ-EOC(2−9−8) and μ-EOC(2−9−12) were precipitated in petroleum ether during purification, while μ-EOC(2−9−2) and μ-EOC(2−9−4) were precipitated in 2-propanol. Since EO(2−9) forms micelles in petroleum ether, unreacted PEE-*b*-PEO precursor would be removed for μ-EOC(2−9−8) and μ-EOC(2−9−12); μ-EOC(2−9−2) and μ-EOC(2−9−4) might contain a small amount of unreacted PEE-*b*-PEO precursor. ^{1}H NMR spectroscopy was used to calculate the composition of μ-EOC (Figure S3, Supporting Information). A summary of the polymers prepared in this study is given in Table 1.

Figure 2a shows a cryo-TEM image of EO(2−9) micelles 10 weeks after their initial preparation by the thin film technique. Spherical micelles were predominantly observed, consistent with the morphology expected from the related PBD-*b*-PEO morphology diagram.[50] The hydrated corona of PEO chains did not

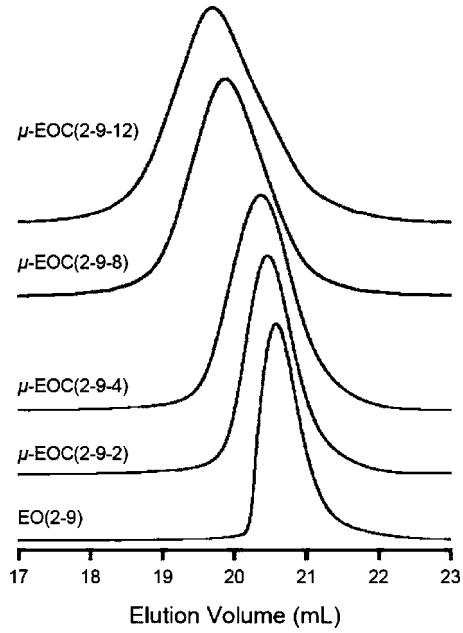

Figure 1. SEC traces of PEE−PEO diblock copolymer precursor and μ-EOC triblocks.

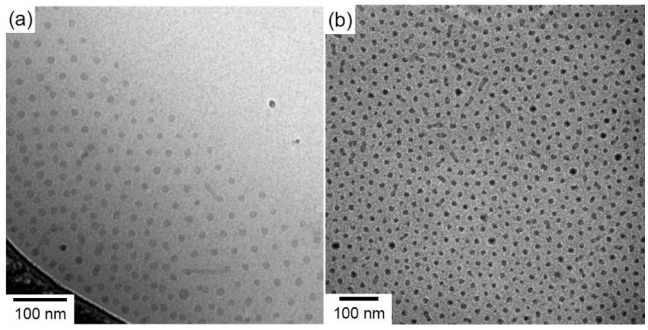

Figure 2. Cryo-TEM images of (a) EO(2−9) and (b) μ-EOC(2−9−2) micelles in 1 wt % aqueous solution after 10 weeks (prepared by the thin film technique).

provide enough contrast for direct observation, although its presence is evident by the approximately hexagonal packing of the micelles. The mean core radius for these micelles, R_{core}, is 6.5 ± 1.5 nm, by averaging more than 100 micelles in cryo-TEM images. This value corresponds to an aggregation number of about 350 based on the known molar mass (2 kg/mol) and density of the PEE block (0.87 g/cm^3).[51] R_{core} of the EO(2−9) micelles is almost comparable to the fully stretched length (FSL) of the E backbone chain (8 nm for 2 kDa) (assuming planar zigzag conformations, where the carbon−carbon (C−C) single bond length is 0.154 nm and the C−C−C bond angle is 109.5°), indicating that the E chains are strongly stretched to decrease the interfacial contact between the PEE and solvated PEO blocks.

Figures 2b, 3, and 4 (as well as Figures S4−S7, Supporting Information) show representative cryo-TEM images of μ-EOC(2−9−x) micelles prepared by the thin film technique after 10 weeks. μ-EOC(2−9−2) self-assembled into spheres and short wormlike micelles in water; however, the micelle cores do not exhibit clear evidence of internal segregation (Figures 2b and S4, Supporting Information). Due to the small difference in electron density between PEE and PMCL, clear contrast in the TEM images may not be evident even if distinct core domains are formed. We also attempted normal TEM imaging of the μ-EOC micelles in an attempt to elucidate their structures. However, drying of these micelles on the TEM grid led to

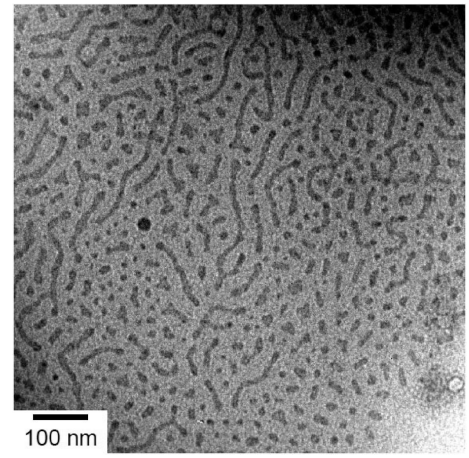

Figure 3. Cryo-TEM image of μ-EOC(2−9−4) micelles in 1 wt % aqueous solution after 10 weeks (prepared by the thin film technique).

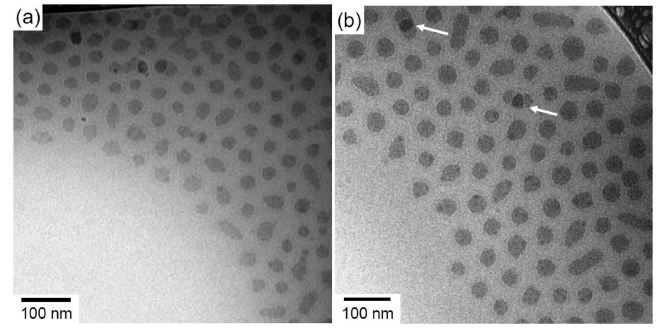

Figure 4. Cryo-TEM images of (a) μ-EOC(2−9−8) and (b) μ-EOC(2−9−12) micelles in 1 wt % aqueous solution after 10 weeks (prepared by the thin film technique). The white arrows highlight what appear to be overlapping micelles.

aggregation phenomena that precluded meaningful interpretation of the images. A variety of morphologies are apparent from the self-assembly of μ-EOC(2−9−4) in water; spheres, Y-junctions, and short wormlike micelles are all evident (Figures 3 and S5, Supporting Information). R_{core} values of μ-EOC(2−9−2) (spheres) and μ-EOC(2−9−4) (cross-sectional radius of worms) are 6.5 ± 1.5 and 5.8 ± 2.0 nm, respectively, comparable to the R_{core} of EO(2−9) micelles. The transition to elongated micelles with increasing fraction of the core blocks is consistent with general trends for both diblocks and miktoarm star terpolymers in water.

Micelles formed from μ-EOC(2−9−8) and μ-EOC(2−9−12) show a majority of irregular spheres or disks with some short wormlike micelles (Figures 4 and S6 and S7, Supporting Information). The increased core contrast due to apparent micelle overlapping (vertical stacking), as indicated by white arrows in Figure 4b, suggests a disklike morphology. The average R_{core} values of μ-EOC(2−9−8) and μ-EOC(2−9−12) micelles are 14.4 ± 4.6 and 17.9 ± 4.9 nm, respectively, much larger than R_{core} for the μ-EOC(2−9−2) and μ-EOC(2−9−4) micelles.

While cryo-TEM enables direct visualization of individual micelles, DLS probes the ensemble behavior and thus provides important information such as the average hydrodynamic radius and distribution of particle size. Normalized squared electric field correlation functions $g_1^2(\tau)$ for EO(2−9) and μ-EOC(2−9−x) micelles are shown in Figure S2, Supporting Information. The decay rate Γ measured at six different scattering angles was linear versus q^2 for all samples; however, the low-q data do not extrapolate to 0 for the μ-EOC(2−9−2) and μ-EOC(2−9−4) samples. A summary of R_h and μ_2/Γ^2

Table 2. DLS Results for μ-EOC Micelles[a]

copolymer	μ_2/Γ^{2b}	$R_h{}^c$ (nm)	$R_h{}^d$ (nm)
EO(2−9)	0.29	37	21, 63
μ-EOC(2−9−2)	0.48	65	27, 112
μ-EOC(2−9−4)	0.40	76	36, 135
μ-EOC(2−9−8)	0.29	68	37, 113
μ-EOC(2−9−12)	0.23	62	37, 98

[a] Formed at a concentration of 1.0 wt % by the thin film technique after 10 weeks. [b] $\theta = 90°$. [c] R_h obtained by fitting correlation functions with the cumulant expansion. [d] R_h obtained by fitting correlation functions with the double-exponential function.

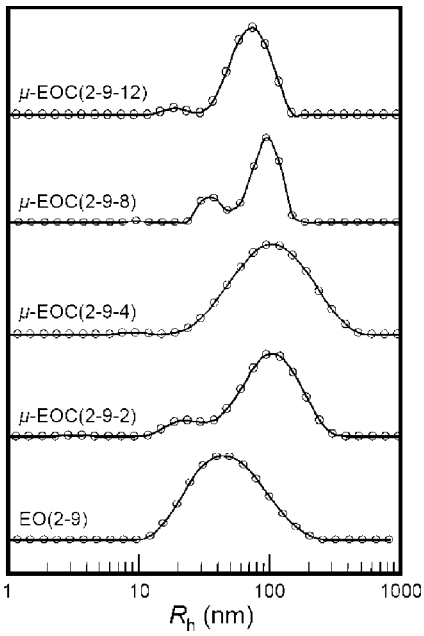

Figure 5. Apparent micelle size distributions of the series of μ-EOC(2−9−x) terpolymers from 1 wt % aqueous micelle solutions (prepared by the thin film technique). The scattering angle is 90°. The solid lines are guides to the eye.

measured from either cumulant or double-exponential fittings is shown in Table 2. The size distributions of these micelles obtained from REPES are also shown in Figure 5.

The broad size distribution for EO(2−9) compared to the typical value for a solution for block copolymer spherical micelles ($\mu_2/\Gamma^2 \leq 0.1$) is attributed to the coexistence of spheres with short wormlike micelles (Figure 2a). This explains why the R_h (37 nm) of EO(2−9) micelles obtained from a cumulant fitting is higher than the average overall micelle radius (21 nm) of EO(2−9) estimated from the cryo-TEM images of the spheres (mean size separation/2). On the other hand, this value (21 nm) is perfectly consistent with the smaller R_h value (21 nm) obtained from double-exponential fits (Table 2). Thus, the R_h values of EO(2−9) from double-exponential fitting (21 and 63 nm) can be attributed to the average sizes of spherical and wormlike micelles, respectively. The mean R_h of μ-EOC(2−9−2) is also larger than that estimated from cryo-TEM images, where spheres having almost the same size as EO(2−9) micelles coexist with short wormlike micelles. The size distribution of μ-EOC(2−9−2) micelles from REPES is bimodal, with peaks corresponding well to the R_h values of 27 and 112 nm obtained from the double-exponential fit. In thicker regions of the vitrified films of μ-EOC(2−9−2) micelles significant overlap was observed (see the darker area in Figure S4, Supporting Information), thus making it difficult to judge the morphology. DLS results for μ-EOC(2−9−4) represent a broad size distribution, reflecting the multiple morphologies including wormlike micelles. For μ-EOC(2−9−8) and μ-EOC(2−9−12) micelles, the average sizes become smaller and the distributions are narrower compared to those of μ-EOC(2−9−4) micelles, whereas R_{core} apparently increases with increasing MCL fraction, as confirmed in the cryo-TEM images. This is consistent with the observed transition from wormlike to either sphere or disklike micelles.

Figure 6 shows cryo-TEM images of μ-EOC(2−9−x) micelles prepared by the dialysis technique. These micellar structures closely correspond to those prepared by the thin film technique. The R_h values between the micelles prepared by the different methods (i.e., dialysis vs thin film techniques) are also similar for all μ-EOC(2−9−x). These results suggest that the micelle transition observed in the current study, from sphere to wormlike to sphere or disk with increasing PMCL chain length, is not dictated by kinetic factors.

Discussion

We now consider three interrelated issues: (i) Are these multicompartment micelles, i.e., are the cores internally segregated? (ii) How are the chains packed within the micelles? (iii) What is the origin of the shape transition from worms to spheres/disks with increasing MCL block size? We also compare these micelles with those documented previously for the μ-EOF system.

The micelle transition from wormlike to sphere/disk with increasing MCL fraction in μ-EOC(2−9−x) implies that the micelles have multicompartment cores. If PEE and PMCL were compatible with each other in the core, this transition would not occur; rather the micelle structures should evolve from spheres to cylinders to bilayers (vesicles) with increasing core fraction, as seen in numerous other polymeric amphiphile systems. Furthermore, polyester and polyolefin blocks should be strongly segregated due to the anticipated large χ, compared to other common block copolymers. We can obtain a plausible estimate for $\chi_{PEE-PMCL}$ using the expression $\chi = 445/T - 0.64$, which was determined for poly(ethylene-*alt*-propylene)-*b*-PLA (PEP-*b*-PLA),[38] a closely related system. Although PEE and PMCL are different from PEP and PLA, they have similar solubility parameters [$\delta_{PEE} = 16.5$,[52] $\delta_{PEP} = 16.0$,[53] $\delta_{PCL} = 19.7$ (PCL = polycaprolactone),[52] and $\delta_{PLA} = 19.7$[53] $J^{1/2}/cm^{3/2}$], assuming $\delta_{PMCL} \approx \delta_{PCL}$ given the minor structural difference. On this basis $\chi N_{PEE-PMCL}$ for μ-EOC(2−9−2) is ca. 36 at 298 K ($\chi = 0.85$ and $N = 42$ on the basis of a 144 Å^3 segment reference volume). This is well above the critical value of $\chi N_{ODT} \approx 10$, where the order−disorder transition (ODT) occurs for a symmetric diblock copolymer,[54] and supports the idea of multicompartment cores of μ-EOC(2−9−x) micelles. Of course, this criterion should not be strictly applied to microphase separation that could be occurring in the core blocks of ABC miktoarm star terpolymer micelles, as it neglects the effects of the number of blocks and the connection of three arms at one junction point.[55] Furthermore, the asymmetry of the core blocks generally leads to $\chi N_{ODT} > 10.5$.[56,57] Therefore, while not definitive, this result should be considered strongly supportive of the formation of multicompartment cores of μ-EOC(2−9−x) micelles.

To experimentally assess the incompatibility between PEE and PMCL, PEE-*b*-PMCL diblock copolymers were prepared by a combination of anionic and ring-opening polymerizations. Two PEE-*b*-PMCL samples having low PDIs were synthesized (SEC and NMR data are shown in Figure S8, Supporting Information) and with molecular weights and compositions comparable to those in the μ-EOC samples. SAXS results for PEE-*b*-PMCL(3−2.7) and PEE-*b*-PMCL(3−16) clearly indicate the formation of bicontinuous gyroid and hexagonally packed cylindrical morphologies, respectively (Figure 7). The microphase-separated structures were retained at 160 °C (although PEE-*b*-PMCL(3−2.7) was disordered at 180 °C). The volume fraction f of PMCL in PEE-*b*-PMCL(3−2.7) is 0.42, estimated

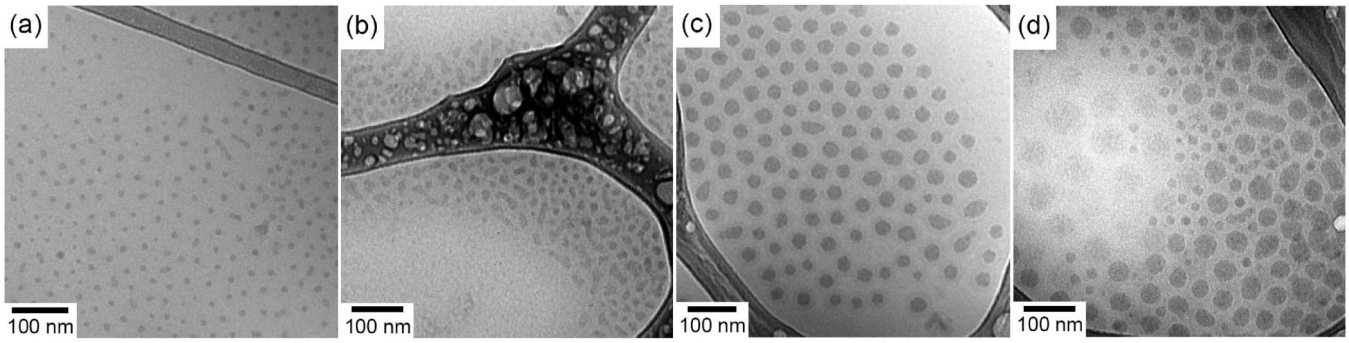

Figure 6. Cryo-TEM images of (a) μ-EOC(2−9−2), (b) μ-EOC(2−9−4), (c) μ-EOC(2−9−8), and (d) μ-EOC(2−9−12) micelles in 0.5 wt % aqueous solution prepared by the dialysis technique after 8−9 weeks.

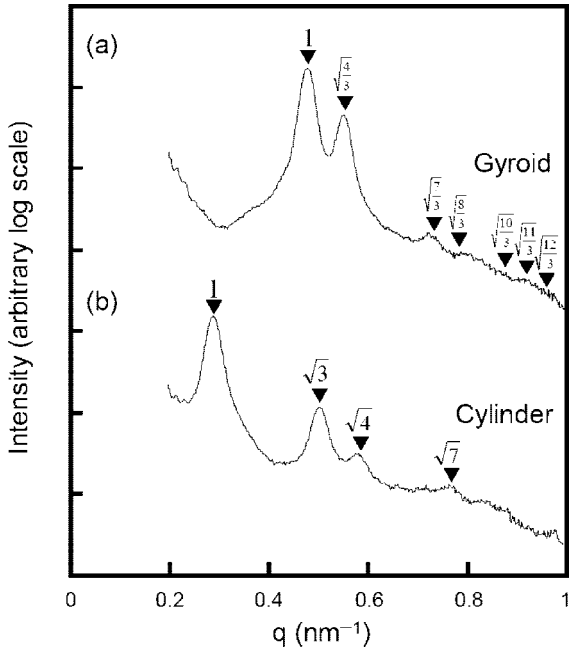

Figure 7. SAXS profiles for (a) PEE-*b*-PMCL(3−2.7) and (b) PEE-*b*-PMCL(3−16) diblock copolymers measured at 25 °C. The numbers after the sample name correspond to the molar masses (kg/mol) of PEE and PMCL blocks, respectively.

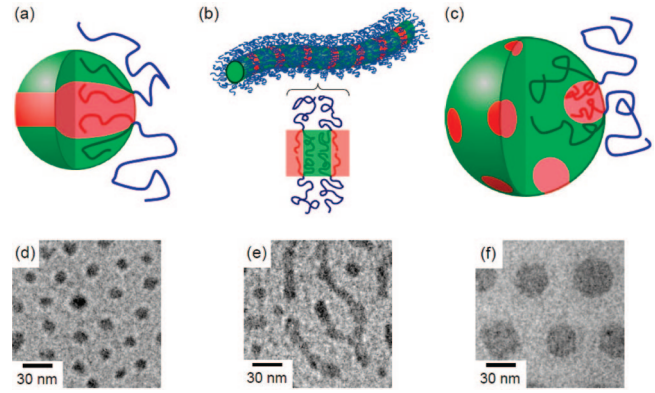

Figure 8. Schematic representation of self-assembled micellar structures of μ-EOC(2−9−x) samples: (a) hamburger micelle, (b) segmented wormlike micelle, and (c) raspberry micelle. Selected cryo-TEM images of (d) μ-EOC(2−9−2), (e) μ-EOC(2−9−4), and (f) μ-EOC(2−9−12) micelles in 1 wt % aqueous solution prepared by the thin film technique after 10 weeks.

using $\rho_{PEE} = 0.87$ g/cm^3 and $\rho_{PMCL} \approx 1.09$ g/cm^3 (assuming $\rho_{PMCL} \approx$ amorphous ρ_{PCL}) at 298 K.[51,58] Using self-consistent mean-field theory, Matsen and Bates located $\chi N_{ODT} = 11$ for a diblock copolymer with $f = 0.42$. Thus, $\chi_{PEE-PMCL}$ is calculated to be 0.16 using $N = 67$ at a T_{ODT} of PEE-*b*-PMCL(3−2.7) of 180 °C. This value is somewhat lower than that estimated for $\chi_{PEP-PLA}$(180 °C) = 0.34, but much large than those other hydrophobic polymer systems (e.g., $\chi_{PS-PI} = 0.03$ and $\chi_{PS-PMMA} = 0.04$ at 180 °C).[39,59] From these combined results, we infer that the μ-EOC micelles have multicompartment cores, even though they cannot be definitely resolved by cryo-TEM.

We previously found that μ-EOF with a relatively long O block formed "hamburger" micelles, in which the superhydrophobic domain of PFPO was sandwiched by two PEE domains as the "buns".[16,34] The O blocks emanating from the PFPO/PEE interfaces curve around the top and bottom of the core to shield the hydrophobic domains from water. In the case of μ-EOC micelles, the relative interfacial tensions γ are expected to be $\gamma_{E/O} > \gamma_{C/O} > \gamma_{E/C}$ [estimated from $\gamma \propto \chi^{0.5} \propto \delta_A - \delta_B$ assuming (i) PEO is well solvated with a water, resulting in a high δ_{PEO}, and (ii) $\delta_{PMCL} \approx \delta_{PCL}$].[52] Thus, we propose the chain packing motif shown in Figure 8a for the μ-EOC(2−9−2) spherical micelles, where an oblate disklike PEE core is sandwiched by two PMCL domains, thereby decreasing interfacial contact between the PEE and the solvated PEO blocks; this is the μ-EOC(2−9−2) version of the "hamburger" micelle. The R_{core} of μ-EOC(2−9−2) (6.5 nm) is only slightly smaller than the FSL of PEE (8.0 nm), consistent with the proposed chain packing motif.

μ-EOC(2−9−4) micelles show a variety of morphologies such as spheres, Y-junctions, and wormlike micelles as shown in Figures 3 and S5, Supporting Information (some micelles showed complicated structures as indicated by a white arrow in Figure S5b, Supporting Information). This coexistence of micelle morphologies is not surprising; a similar coexistence of micellar structures was observed for μ-EOF micelles in water.[32] It has been well documented that attaining equilibrium is impeded by slow unimer exchange between micelles in water due to the extremely low critical micelle concentration, which nearly eliminates the presence of free chains in solution.[60,61] Thus, the micelles of various sizes cannot equilibrate to a single preferred size or shape. Polydispersity of the constituent polymer molecules might also contribute to the coexistence of the morphologies.[62] The slight reduction in R_{core} for the wormlike μ-EOC(2−9−4) micelles compared to the hamburger micelles of μ-EOC(2−9−2) is consistent with similar reductions in R_{core} commonly observed upon transitioning from spherical to wormlike to bilayer micelles in other polymeric amphiphile systems.[44,61]

The wormlike micelles observed in solutions of μ-EOC(2−9−4) are likely to be segmented as shown in Figure 8b, as R_{core} of the wormlike micelles is comparable to (but slightly smaller than) the R_{core} of EO(2−9) and μ-EOC(2−9−2) micelles. In a segmented wormlike micelle, PEE and PMCL cores would

alternately be stacked along the axis of a cylinder and PEO chains would emanate from the PEE/PMCL interfaces to protect the whole micelle core. We previously observed segmented wormlike structure in related μ-EOF(2−9−3.5) micelles (in coexistence with several Y-junctions), where the F and E phases are alternately stacked along the axis of a cylinder.[32]

Further increasing the MCL fraction resulted in the transition from wormlike to either sphere or disklike morphologies for μ-EOC(2−9−8) and μ-EOC(2−9−12) micelles (Figure 4). Nonionic disklike micelles consisting of random coil blocks were recently found in another system and visualized by cryo-TEM.[10,63] The formation of disklike structures implies that the system lies in the SSSR, and the overwhelming interfacial tension between the core and solvated corona blocks leads to fully stretched core blocks, thus minimizing interfacial contact between the core and corona blocks; a flat circular disk results. Cryo-TEM images of such disklike micelles often exhibit the circular cores of the micelles; "edge-on" views are rarely observed,[64] likely due to in-plane orientation of the micelles during the blotting process.[63] To distinguish disklike micelles and large spherical micelles that would give similar circular features, the FSL of the core blocks can be compared to the radius of the features. In the case of μ-EOC(2−9−12) micelles, the observed R_{core} of 17.9 nm is well below 78 nm, the FSL of a PMCL block (assuming a C−O single bond length of 0.139 nm and a C−O−C bond angle of 107°), thus supporting the possibility of spherical micelles. No edge-on structures of the micelles were observed for either μ-EOC(2−9−8) or μ-EOC-(2−9−12). Given that the segregation strength between PMCL and PEE is moderate (i.e., far from the SSSR regime), we suggest that the structures are probably more or less spherical. However, the R_{core} values of μ-EOC(2−9−8) and μ-EOC(2−9−12) micelles (14.4 and 17.9 nm) do exceed the FSL of the PEE block (8 nm). Therefore, the PEE domains would likely form isolated patches dispersed in a PMCL matrix (raspberry-like micelles as illustrated in Figure 8c), rather than hamburger and three- or four-lobe multicompartment micelles. A similar transition has been observed in related μ-EOF samples.[32] Namely, segmented wormlike μ-EOF(2−9−3.5) micelles transformed to multicompartmentalized raspberry-like micelles and multicompartment worms in μ-EOF(2−9−5) samples; larger F blocks in μ-EOF(2−9−5) form the matrix of the sphere or cylinder, while the E blocks form isolated patches. Thus, the fact that the core chain lengths for μ-EOC(2−9−8) and μ-EOC(2−9−12) are more asymmetric than that for μ-EOF(2−9−5) supports the formation of raspberry-like morphology in μ-EOC(2−9−8) and μ-EOC(2−9−12) micelles.

What is the origin of the transition from segmented wormlike to spherical raspberry-like micelles with increasing MCL (core) fraction in μ-EOC(2−9−x)? The PMCL block has a lower interfacial tension with water than PEE, and thus, the PEE blocks would prefer to minimize contact with the hydrated PEO chains. For diblocks, the micelle morphology sequence with block composition depends mainly on the core/corona interfacial tension ($\gamma_{core/corona}$) and the total molecular weight for a dilute system (although the polymer concentration can also play a role[65,66]).[50] With decreasing $\gamma_{core/corona}$ or increasing molecular weight, the composition window for each morphology shifts to lower values of w_{corona}. For example, spherical PB−PEO micelles evolve to worms at $w_{PEO} \approx 0.5-0.6$,[50] whereas the same transition occurs at $w_{PEO} \approx 0.3-0.4$ for the less strongly segregated PMCL−PEO micelles.[43] w_{PEO} for μ-EOC(2−9−12) is 0.39, which corresponds to the onset of the spherical to wormlike micelle transition for PMCL−PEO micelles; at $w_{PEO} < 0.39$ wormlike micelles or vesicles are observed for dilute aqueous dispersions of PMCL−PEO. Thus, PMCL and PEO chains of μ-EOC(2−9−8) ($w_{PEO} = 0.47$) and μ-EOC(2−9−12) would favor predominantly spherical micelles rather than wormlike micelles if the minority PEE domains do not dictate the overall micelle shape. This assumption seems reasonable given that the low volume fraction PEE domains should be isolated from each other in the PMCL matrix.

Conclusions

We have prepared a set of well-defined μ-EOC star triblock copolymers and reported their self-assembly as dilute dispersions in water. Cryo-TEM measurements, supported by DLS, revealed that the self-assembly of μ-EOC micelles evolves from spheres to worms with increasing MCL fraction. Further increasing the MCL fraction showed a transition from wormlike micelles back to spherical or disk-like structures. The electron density contrast between the PMCL and PEE blocks was insufficient for definitive evidence of multicompartmented cores by cryo-TEM. However, SAXS analysis of PEE−PMCL diblock copolymers having molecular weights comparable to those of the core blocks in the μ-EOC samples showed ordered structures, supporting the conclusion that the micelle cores are indeed internally segregated in the micelles.

Acknowledgment. This work was supported by the National Science Foundation (NSF) through the University of Minnesota MRSEC, Award DMR-0212302. Parts of this work were carried out in the University of Minnesota I.T. Characterization Facility, which receives partial support from the NSF through the NNIN program. We thank John Zupancich for his assistance with μ-EOC preparation and for fruitful discussions. We appreciate the assistance of Dr. Ozan Ugurlu with some of the TEM measurements.

Supporting Information Available: Figures giving the synthetic route to PEE−PMCL block copolymers, normalized squared correlation functions for μ-EOC(2−9−x) terpolymers, ^{1}H NMR spectra of PEE−PEO(2−9), μ-EOC(2−9−2), PEE−OH(3K), and PEE-*b*-PMCL(3−2.7), cryo-TEM images of μ-EOC(2−9−2), μ-EOC(2−9−4), μ-EOC(2−9−8), and μ-EOC(2−9−12) micelles, and SEC traces of PEE−OH(3K), PEE-*b*-PMCL(3−2.7), and PEE-*b*-PMCL(3−16). This material is available free of charge via the Internet at http://pubs.acs.org.

References and Notes

(1) Li, Z. B.; Kesselman, E.; Talmon, Y.; Hillmyer, M. A.; Lodge, T. P. *Science* **2004**, *306*, 98–101.
(2) Laschewsky, A. *Curr. Opin. Colloid Interface Sci.* **2003**, *8*, 274–281.
(3) Lutz, J. F.; Laschewsky, A. *Macromol. Chem. Phys.* **2005**, *206*, 813–817.
(4) Lodge, T. P.; Rasdal, A.; Li, Z. B.; Hillmyer, M. A. *J. Am. Chem. Soc.* **2005**, *127*, 17608–17609.
(5) Yu, G. E.; Eisenberg, A. *Macromolecules* **1998**, *31*, 5546–5549.
(6) Gohy, J. F.; Willet, N.; Varshney, S.; Zhang, J. X.; Jerome, R. *Angew. Chem., Int. Ed.* **2001**, *40*, 3214–3216.
(7) Lei, L. C.; Gohy, J. F.; Willet, N.; Zhang, J. X.; Varshney, S.; Jerome, R. *Macromolecules* **2004**, *37*, 1089–1094.
(8) Lei, L. C.; Gohy, J. F.; Willet, N.; Zhang, J. X.; Varshney, S.; Jerome, R. *Polymer* **2004**, *45*, 4375–4381.
(9) Lei, L. C.; Gohy, J. F.; Willet, N.; Zhang, J. X.; Varshney, S.; Jerome, R. *Polymer* **2006**, *47*, 2723–2727.
(10) Zhou, Z. L.; Li, Z. B.; Ren, Y.; Hillmyer, M. A.; Lodge, T. P. *J. Am. Chem. Soc.* **2003**, *125*, 10182–10183.
(11) Pochan, D. J.; Chen, Z. Y.; Cui, H. G.; Hales, K.; Qi, K.; Wooley, K. L. *Science* **2004**, *306*, 94–97.
(12) Li, Z. B.; Chen, Z. Y.; Cui, H. G.; Hales, K.; Qi, K.; Wooley, K. L.; Pochan, D. J. *Langmuir* **2005**, *21*, 7533–7539.
(13) Chen, Z. Y.; Cui, H. G.; Hales, K.; Li, Z. B.; Qi, K.; Pochan, D. J.; Wooley, K. L. *J. Am. Chem. Soc.* **2005**, *127*, 8592–8593.
(14) Cui, H. G.; Chen, Z. Y.; Wooley, K. L.; Pochan, D. J. *Macromolecules* **2006**, *39*, 6599–6607.
(15) Cui, H. G.; Chen, Z. Y.; Zhong, S.; Wooley, K. L.; Pochan, D. J. *Science* **2007**, *317*, 647–650.
(16) Li, Z. B.; Chen, Z. Y.; Cui, H. G.; Hales, K.; Wooley, K. L.; Pochan, D. J. *Langmuir* **2007**, *23*, 4689–4694.

(17) Kubowicz, S.; Baussard, J. F.; Lutz, J. F.; Thunemann, A. F.; von Berlepsch, H.; Laschewsky, A. *Angew. Chem., Int. Ed.* **2005**, *44*, 5262–5265.
(18) Thunemann, A. F.; Kubowicz, S.; von Berlepsch, H.; Mohwald, H. *Langmuir* **2006**, *22*, 2506–2510.
(19) Lambert, O.; Reutenauer, S.; Hurtrez, G.; Riess, G.; Dumas, P. *Polym. Bull.* **1998**, *40*, 143–149.
(20) Fujimoto, T.; Zhang, H. M.; Kazama, T.; Isono, Y.; Hasegawa, H.; Hashimoto, T. *Polymer* **1992**, *33*, 2208–2213.
(21) Iatrou, H.; Hadjichristidis, N. *Macromolecules* **1992**, *25*, 4649–4651.
(22) Sioula, S.; Tselikas, Y.; Hadjichristidis, N. *Macromolecules* **1997**, *30*, 1518–1520.
(23) Bellas, V.; Iatrou, H.; Hadjichristidis, N. *Macromolecules* **2000**, *33*, 6993–6997.
(24) Lambert, O.; Dumas, P.; Hurtrez, G.; Riess, G. *Macromol. Rapid Commun.* **1997**, *18*, 343–351.
(25) Nasser-Eddine, M.; Reutenauer, S.; Delaite, C.; Hurtrez, G.; Dumas, P. *J. Polym. Sci., Part A: Polym. Chem.* **2004**, *42*, 1745–1751.
(26) Feng, X. S.; Pan, C. Y. *Macromolecules* **2002**, *35*, 4888–4893.
(27) Feng, X. S.; Pan, C. Y. *Macromolecules* **2002**, *35*, 2084–2089.
(28) He, T.; Li, D. J.; Sheng, X.; Zhao, B. *Macromolecules* **2004**, *37*, 3128–3135.
(29) Hadjichristidis, N.; Iatrou, H.; Pitsikalis, M.; Pispas, S.; Avgeropoulos, A. *Prog. Polym. Sci.* **2005**, *30*, 725–782.
(30) Li, Z. B.; Hillmyer, M. A.; Lodge, T. P. *Macromolecules* **2004**, *37*, 8933–8940.
(31) Wang, G.; Huang, J. *J. Polym. Sci., Part A: Polym. Chem.* **2008**, *46*, 1136–1150.
(32) Li, Z. B.; Hillmyer, M. A.; Lodge, T. P. *Langmuir* **2006**, *22*, 9409–9417.
(33) Li, Z. B.; Hillmyer, M. A.; Lodge, T. P. *Nano Lett.* **2006**, *6*, 1245–1249.
(34) Li, Z. B.; Hillmyer, M. A.; Lodge, T. P. *Macromolecules* **2006**, *39*, 765–771.
(35) Semenov, A. N.; Nyrkova, I. A.; Khokhlov, A. R. *Macromolecules* **1995**, *28*, 7491–7500.
(36) Geng, Y.; Discher, D. E. *Polymer* **2006**, *47*, 2519–2525.
(37) Zalusky, A. S.; Olayo-Valles, R.; Wolf, J. H.; Hillmyer, M. A. *J. Am. Chem. Soc.* **2002**, *124*, 12761–12773.
(38) Schmidt, S. C.; Hillmyer, M. A. *J. Polym. Sci., Part B: Polym. Chem.* **2002**, *40*, 2364–2376.
(39) Frielinghaus, H.; Hermsdorf, N.; Almdal, K.; Mortensen, K.; Messe, L.; Corvazier, L.; Fairclough, J. P. A.; Ryan, A. J.; Olmsted, P. D.; Hamley, I. W. *Europhys. Lett.* **2001**, *53*, 680–686.
(40) Pangborn, A. B.; Giardello, M. A.; Grubbs, R. H.; Rosen, R. K.; Timmers, F. J. *Organometallics* **1996**, *15*, 1518–1520.
(41) Trollsas, M.; Kelly, M. A.; Claesson, H.; Siemens, R.; Hedrick, J. L. *Macromolecules* **1999**, *32*, 4917–4924.
(42) Vangeyte, P.; Jerome, R. *J. Polym. Sci., Part A: Polym. Chem.* **2004**, *42*, 1132–1142.
(43) Zupancich, J. A.; Bates, F. S.; Hillmyer, M. A. *Macromolecules* **2006**, *39*, 4286–4288.
(44) Zhang, L. F.; Eisenberg, A. *J. Am. Chem. Soc.* **1996**, *118*, 3168–3181.
(45) Hillmyer, M. A.; Bates, F. S. *Macromolecules* **1996**, *29*, 6994–7002.
(46) Bellare, J. R.; Davis, H. T.; Scriven, L. E.; Talmon, Y. *J. Electron Microsc. Tech.* **1988**, *10*, 87–111.
(47) Koppel, D. E. *J. Chem. Phys.* **1972**, *57*, 4814–4820.
(48) Frisken, B. J. *Appl. Opt.* **2001**, *40*, 4087–4091.
(49) Jakes, J. *Collect. Czech. Chem. Commun.* **1995**, *60*, 1781–1797.
(50) Jain, S.; Bates, F. S. *Science* **2003**, *300*, 460–464.
(51) Fetters, L. J.; Lohse, D. J.; Richter, D.; Witten, T. A.; Zirkel, A. *Macromolecules* **1994**, *27*, 4639–4647.
(52) Ruzette, A. V. G.; Mayes, A. M. *Macromolecules* **2001**, *34*, 1894–1907.
(53) Van Krevelen, D. W. *Properties of Polymers*; Elsevier: New York, 1997; Chapter 7, pp 189−220.
(54) Leibler, L. *Macromolecules* **1980**, *13*, 1602–1617.
(55) Floudas, G.; Hadjichristidis, N.; Iatrou, H.; Pakula, T.; Fischer, E. W. *Macromolecules* **1994**, *27*, 7735–7746.
(56) Khandpur, A. K.; Forster, S.; Bates, F. S.; Hamley, I. W.; Ryan, A. J.; Bras, W.; Almdal, K.; Mortensen, K. *Macromolecules* **1995**, *28*, 8796–8806.
(57) Matsen, M. W.; Bates, F. S. *Macromolecules* **1996**, *29*, 1091–1098.
(58) Perret, R.; Skoulios, A. *Makromol. Chem.* **1972**, *156*, 157.
(59) Russell, T. P.; Hjelm, R. P.; Seeger, P. A. *Macromolecules* **1990**, *23*, 890–893.
(60) Won, Y. Y.; Davis, H. T.; Bates, F. S. *Macromolecules* **2003**, *36*, 953–955.
(61) Jain, S.; Bates, F. S. *Macromolecules* **2004**, *37*, 1511–1523.
(62) Terreau, O.; Luo, L. B.; Eisenberg, A. *Langmuir* **2003**, *19*, 5601–5607.
(63) Edmonds, W. F.; Li, Z. B.; Hillmyer, M. A.; Lodge, T. P. *Macromolecules* **2006**, *39*, 4526–4530.
(64) Lodge, T. P.; Hillmyer, M. A.; Zhou, Z. *Macromolecules* **2004**, *37*, 6680–6682.
(65) Discher, D. E.; Eisenberg, A. *Science* **2002**, *297*, 967–973.
(66) Simone, P. M.; Lodge, T. P. *Macromolecules* **2008**, *41*, 1753–1759.

MA801001S